Progress In Electromagnetics Research, PIER 42, 173–192, 2003

WAVE PROPAGATION IN A CURVED WAVEGUIDE WITH ARBITRARY DIELECTRIC TRANSVERSE PROFILES

Z. Menachem

Department of Solid Mechanics, Materials and Structures
Faculty of Engineering
Tel-Aviv University
Ramat Aviv 69978, Israel

Abstract—A rigorous approach is derived for the analysis of electromagnetic (EM) wave propagation in dielectric waveguides with arbitrary profiles, situated inside rectangular metal tubes, and along a curved dielectric waveguide. The first objective is to develop a mode model in order to provide a numerical tool for the calculation of the output fields for radius of curvature $0.1\,\mathrm{m} \leq R \leq \infty$. Therefore we take into account all the terms in the calculations, without neglecting the terms of the bending. Another objective is to demonstrate the ability of the model to solve practical problems with inhomogeneous dielectric profiles. The method is based on Fourier coefficients of the transverse dielectric profile and those of the input wave profile. These improvements contribute to the application of the model for inhomogeneous dielectric profiles with single or multiple maxima in the transverse plane. This model is useful for the analysis of dielectric waveguides in the microwave and the millimeter-wave regimes, for diffused optical waveguides in integrated optics, and for IR regimes.

1. INTRODUCTION

Dielectric-coated metallic waveguide have attracted a considerable interest in a wide variety of transverse profiles. Various methods for the analysis of similar problems, of wave propagation in dielectric inhomogeneous waveguides, have been studied in the literature. The propagation of general-order modes in curved rectangular waveguide examined by using asymptotic expansion method [1]. A matrix formulation of the generalized telegraphist's equation [2] used to obtain a general set of equations for a guide of arbitrary cross-section with curved axis. The matrix elements involved mode-coupling coefficients which were obtained as rather general integrals of the mode basis functions and the space variables. Asymptotic forms of the coupling coefficients for gentle bends were determined and applied to propagation in rectangular guide bent into an arc of a circle between two sections of straight guide. The results include the junction reflection and the propagation coefficients as the first term in a series of inverse powers in the radius of curvature of the bend. For very sharp bends the matrix equations are tackled directly and results calculated numerically by truncation of the matrices at third order. By comparison with truncation at first and second order it seems that third order truncation should yield accurate numerical results. The asymptotic results were quite good even for radius of curvature of the guide center line as small as the guide width.

Slabs with more general refractive index distributions were considered by Heiblum and Harris [3] and by Kawakami, Miyagi and Nishida [4], using a WKB method [5]. These two papers consider the case when the mode on the curved waveguide is not a small perturbation of a mode on the straight guide, but was guided essentially by the outer boundary. The modes of this nature are known as "edge-guided" modes. The increase in radiation losses due to curvature for slightly leaky modes on hollow dielectric or imperfect metallic waveguides, a sort of composite of open and closed waveguide behavior, was investigated by Marcatily and Schmeltzer [6].

Several methods of investigation of propagation were developed for study of empty curved waveguide and bends [7–10]. The results of precise numerical computations and extensive analytical investigation of the angular propagation constants were presented for various electromagnetic modes which may exit in waveguide bends of rectangular cross section [7]. A new equivalent circuit for circular E-plane bends, suitable for any curvature radius and rectangular waveguide type was presented in Ref. [8]. An accurate and efficient method of moments solution together with a mode-matching technique

for the analysis of curved bends in a general parallel-plate waveguide was described in the case of a rectangular waveguides [9]. A rigorous differential method describing the propagation of an electromagnetic wave in a bent waveguide was presented in Ref. [10].

An extensive survey of the related literature can be found in the book on electromagnetic waves and curved structures [11]. Propagation in curved rectangular waveguides by the perturbation techniques was introduced for a guide of cross-section $a \times b$ whose axis was bent to radius R. Likewise, the twisted coordinate system with application to rectangular waveguides was introduced in Ref. [11]. The other chapters were concerned with curved guides, both rectangular and circular. Calculations were performed for the propagation coefficient, reflection, mode-conversion, mode-coupling and eigenfunctions for a variety of configurations by the asymptotic method. The radiation from curved open structures is mainly considered by using a perturbation approach, that is by treating the curvature as a small perturbation of the straight configuration. The perturbational approach is not entirely suited for the analysis of relatively sharp bends, such as those required in integrated optics and especially short millimeter waves.

The models based on the perturbation theory solve problems only for a large radius of curvature ($R \to \infty$). The objective of this work was to generalize the method in Ref. [12] also for a curved dielectric waveguide. The mode model provides us a numerical tool for the calculation of the output fields and power density for radius of curvature $0.1\,\mathrm{m} \leq R \leq \infty$. Therefore we take into account all the terms in the calculations, without neglecting the terms of the bending (namely, up to the fourth order of $1/R$, where the further orders are equal zero). This means that we have polynomial expressions of order four. The calculations are depended on h_ζ, h_ζ^2, h_ζ^3 and h_ζ^4 ($h_\zeta = 1 + x/R$), where h_ζ is the metric coefficient. Thus the maximum value of the bending is of the order of $1/R^4$. This will enable us to understand more precisely the influence of the bending on the output fields, output power density, and output power transmission in the case of arbitrary dielectric profiles. Ref. [12] was especially applicable for continuous problems (i.e., smoothly varying profiles). Thus the another objective is to demonstrate the ability of the model to solve practical problems with inhomogeneous dielectric profiles. This theoretical model has been applied in the case of a curved rectangular waveguides with arbitrary dielectric transverse profiles in the mm-waves regime. The purpose of this study was to develop transfer relations between the wave components at the output and input ports of such waveguides as matrix functions of their dielectric profiles. The following sections

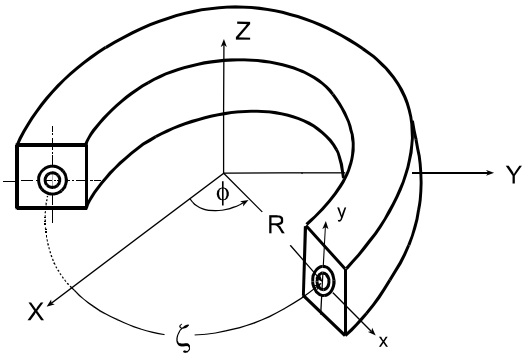

Figure 1. The curved coordinate system (x, y, ζ).

present the formulation and the derivation of this method for a curved rectangular waveguides with arbitrary dielectric profiles.

2. FORMULATION OF THE PROBLEM

The system (x, y, ζ) in conjunction with the curved rectangular waveguide is shown in Fig. 1. The curved waveguide transformation of the coordinates is given by

$$X = (R + x)\cos\left(\frac{\zeta}{R}\right) , \tag{1a}$$

$$Y = (R + x)\sin\left(\frac{\zeta}{R}\right) , \tag{1b}$$

$$Z = y . \tag{1c}$$

In this curved system the metric coefficients are:

$$h_x = 1, \qquad h_y = 1, \qquad h_\zeta = 1 + \frac{x}{R} \tag{2a, b, c}$$

and a differential length is given by $ds^2 = h_x^2 dx^2 + h_y^2 dy^2 + h_\zeta^2 d\zeta^2$, where R is the bending radius of the waveguide. Further the bending radius is defined as the mean radius (Fig. 1) of the curved waveguide. A cross section of the curved waveguide in the regions $0 \le x \le a$ and $0 \le y \le b$ is shown in Fig. 1, where a and b are the dimensions in the cross-section. The case for the straight waveguide is obtained by letting $R \to \infty$.

The derivation is based on Maxwell's equations for the computation of output fields, output power density, and output power

transmission at each point during propagation through a curved waveguide. The method is based on Fourier coefficients of the transverse dielectric profile and those of the input wave profile. Thus the accuracy of the method is depended on the number of the modes in the system. This model is applied to solve problems of arbitrary profiles (continuous and discontinuous dielectric profiles). The comparison between this method for the wave propagation in uniform curved waveguide with a rectangular cross section and the method for the propagation in uniform curved waveguide with a circular cross section [13] will be given after the derivation.

3. THE DERIVATION

In this derivation we present an extension of the transfer matrix function (TMF) technique [12] for the analysis of wave propagation in uniform curved waveguide regions with arbitrary dielectric transverse profile. The objective is to develop a mode model in order to provide a numerical tool for the calculation of the output fields, output power density, and output power transmission for radius of curvature $0.1\,\mathrm{m} \leq R \leq \infty$. Therefore we take into account all the terms in the calculations, without neglecting the terms of the bending.

The wave equations for the electric and magnetic field components in the inhomogeneous dielectric medium $\epsilon(x, y)$ are given by

$$\nabla^2 \boldsymbol{E} + \omega^2 \mu \epsilon \boldsymbol{E} + \nabla \left(\boldsymbol{E} \cdot \frac{\nabla \epsilon}{\epsilon} \right) = 0, \tag{3a}$$

and

$$\nabla^2 \boldsymbol{H} + \omega^2 \mu \epsilon \boldsymbol{H} + \frac{\nabla \epsilon}{\epsilon} \times (\nabla \times \boldsymbol{H}) = 0, \tag{3b}$$

respectively. The transverse dielectric profile is defined as

$$\epsilon(x, y) = \epsilon_0 \left[1 + \chi_o g(x, y) \right], \tag{4}$$

where ϵ_0 represents the vacuum dielectric constant, χ_o is the susceptibility of the dielectric material and $g(x, y)$ is its profile function in the waveguide.

The normalized transverse derivatives of the dielectric profile $g(x, y)$ are defined as

$$g_x \equiv \frac{1}{\epsilon(x, y)} \left[\frac{\partial}{\partial x} \epsilon(x, y) \right], \qquad g_y \equiv \frac{1}{\epsilon(x, y)} \left[\frac{\partial}{\partial y} \epsilon(x, y) \right]. \tag{5a, b}$$

From the transformation of Eqs. (1a), (1b), and (1c) one can derive the *exact Laplacian*, and obtain the wave equations for the electric and magnetic field in the inhomogeneous dielectric medium.

The components of the *exact Laplacian* are given by

$$(\nabla^2 \boldsymbol{E})_x = \nabla^2 E_x - \frac{1}{R^2 h_\zeta^2} E_x - 2\frac{1}{R h_\zeta^2}\frac{\partial}{\partial \zeta} E_\zeta, \tag{6a}$$

$$(\nabla^2 \boldsymbol{E})_y = \nabla^2 E_y, \tag{6b}$$

$$(\nabla^2 \boldsymbol{E})_\zeta = \nabla^2 E_\zeta - \frac{1}{R^2 h_\zeta^2} E_\zeta + 2\frac{1}{R h_\zeta^2}\frac{\partial}{\partial \zeta} E_\zeta, \tag{6c}$$

where

$$\nabla^2 = \frac{\partial^2}{\partial x^2} + \frac{\partial^2}{\partial y^2} + \frac{1}{h_\zeta^2}\frac{\partial^2}{\partial \zeta^2} + \frac{1}{R h_\zeta}\frac{\partial^2}{\partial x}. \tag{7}$$

The wave equations (3a) and (3b) are written in the form

$$(\nabla^2 \boldsymbol{E})_i + k^2 E_i + \partial_x (E_x g_x + E_y g_y) = 0, \tag{8a, b, c}$$

$$(\nabla^2 \boldsymbol{H})_i + k^2 H_i + \partial_x (H_x g_x + H_y g_y) = 0, \tag{8d, e, f}$$

where $i = x, y$. The local wavenumber parameter is given by $k = \omega\sqrt{\mu\epsilon(x,y)} = k_0\sqrt{1+\chi_o g(x,y)}$, and the free-space wavenumber is given by $k_0 = \omega\sqrt{\mu_0\epsilon_0}$. The expression $(\nabla^2 \boldsymbol{E})_x$, for instance, is given according to Eq. (6a).

The transverse Laplacian operator is defined as

$$\nabla_\perp^2 = \nabla^2 - \frac{1}{h_\zeta^2}\frac{\partial^2}{\partial \zeta^2}, \tag{9}$$

where $h_\zeta^2 = (1 + x/R)^2$.

The Laplace transform

$$\tilde{a}(s) = \mathcal{L}\{a(\zeta)\} \int_{\zeta=0}^{\infty} a(\zeta) e^{-s\zeta} d\zeta, \tag{10}$$

is applied on the ζ-dimension, where $a(\zeta)$ represents any ζ-dependent variables and $\zeta = R\ \phi$.

By using Laplace transform the fields at $\zeta = \infty$ are zero. Therefore the ζ axis of the curved waveguide is a rectangular *helix* with a small step's angle and the metric coefficients as given in Eqs. (2a) to (2c) are justified (see Appendix A). The model in this paper can take into

account the cases of smaller R only if the step's angle (δ_p) is very small, where the condition is given in Appendix A.

By substitution of Eqs. (6a), (6b) and (6c) into Eqs. (8a), (8b) and (8c), using Laplace transform, and multiply by h_ζ^2, Eqs. (3a) are described in s-plane in the form

$$h_\zeta^2\left(\nabla_\perp^2+\frac{s^2}{h_\zeta^2}+k^2\right)\tilde{E}_x+h_\zeta^2\partial_x\left(\tilde{E}_x g_x+\tilde{E}_y g_y\right)+h_\zeta\frac{1}{R}\partial_x\left(\tilde{E}_x\right)-\frac{1}{R^2}\tilde{E}_x-\frac{2}{R}s\tilde{E}_\zeta = \left(sE_{x_0}+E'_{x_0}\right)-\frac{2}{R}E_{\zeta_0}, \tag{11a}$$

$$h_\zeta^2\left(\nabla_\perp^2+\frac{s^2}{h_\zeta^2}+k^2\right)\tilde{E}_y+h_\zeta^2\partial_y\left(\tilde{E}_x g_x+\tilde{E}_y g_y\right)+h_\zeta\frac{1}{R}\partial_x\left(\tilde{E}_y\right) = \left(sE_{y_0}+E'_{y_0}\right), \tag{11b}$$

$$h_\zeta^2\left(\nabla_\perp^2+\frac{s^2}{h_\zeta^2}+k^2\right)\tilde{E}_\zeta+sh_\zeta^2\left(\tilde{E}_x g_x+\tilde{E}_y g_y\right)+h_\zeta\frac{1}{R}\partial_x\left(\tilde{E}_\zeta\right)-\frac{1}{R^2}\tilde{E}_\zeta+\frac{2}{R}s\tilde{E}_\zeta = \left(sE_{\zeta_0}+E'_{\zeta_0}\right)+\frac{2}{R}E_{\zeta_0}+h_\zeta^2\left(E_{x_0}g_x+E_{y_0}g_y\right), \tag{11c}$$

where the transverse Laplacian operator is defined according to Eq. (9), E_{x_0}, E_{y_0}, E_{ζ_0} are the initial values of the corresponding fields at $\zeta=0$, i.e., $E_{x_0}=E_x(x,y,\zeta=0)$ and $E'_{x_0}=\frac{\partial}{\partial\zeta}E_x(x,y,\zeta)|_{\zeta=0}$.

A Fourier transform is applied on the transverse dimension

$$\bar{g}(k_x,k_y)=\mathcal{F}\{g(x,y)\}=\int_x\int_y g(x,y)e^{-jk_xx-jk_yy}dxdy, \tag{12}$$

and the differential equation (11a) is transformed to an algebraic form in the (ω,s,k_x,k_y) space, as follows

$$k_\zeta^2\bar{\tilde{E}}_x+s^2\bar{\tilde{E}}_x+k_o^2\chi_o\bar{g}*\bar{\tilde{E}}_x+jk_x\left(\bar{g}_x*\bar{\tilde{E}}_x+\bar{g}_y*\bar{\tilde{E}}_y\right)-\frac{1}{R^2}\bar{\tilde{E}}_x-\frac{2}{R}s\bar{\tilde{E}}_\zeta + \bar{q}_\zeta*\left(k_\zeta^2\right)\bar{\tilde{E}}_x+k_o^2\chi_o\bar{q}_\zeta*\left(\bar{g}*\bar{\tilde{E}}_x\right)+j\bar{q}_\zeta*\left[k_x\left(\bar{g}_x*\bar{\tilde{E}}_x+\bar{g}_y*\bar{\tilde{E}}_y\right)\right] + \frac{1}{R}\left(jk_x\right)\bar{\tilde{E}}_x+\frac{1}{R}j\bar{p}_\zeta*\left(k_x\bar{\tilde{E}}_x\right)=\left(s\bar{E}_{x_0}+\bar{E}'_{x_0}\right)-\frac{1}{sR}\left(s\bar{E}_{\zeta_0}+\bar{E}'_{\zeta_0}\right), \tag{12a}$$

where $k_\zeta=\sqrt{k_o^2-k_x^2-k_y^2}$. Similarly, the other differential equations are obtained. The asterisk symbol denotes the convolution operation

$$\bar{g}*\bar{E}=\mathcal{F}\{g(x,y)E(x,y)\}.$$

The metric coefficient h_ζ is a function of x, thus we defined

$$h_\zeta = 1 + p_\zeta(x), \qquad p_\zeta(x) = x/R, \tag{13a, b}$$

$$h_\zeta^2 = 1 + q_\zeta(x), \qquad q_\zeta(x) = (2/R)x + (1/R^2)x^2. \tag{13c, d}$$

The method of images is applied to satisfy the conditions $\widehat{n} \times E = 0$ and $\widehat{n} \cdot (\nabla \times E) = 0$ on the surface of the ideal metallic waveguide walls, where $\widehat{n}$ is a unit vector perpendicular to the surface. The technique for the computation of the boundary conditions by using the method of images was described in detail in Ref. [12]. The metric coefficient h_ζ is a function of x (Eqs. (13a) to (13d)).

Thus the elements of the matrices $\mathbf{P^{(0)}}$ and $\mathbf{Q^{(0)}}$ are defined as:

$$\bar{p}^{(o)}_{\zeta_{(n,m)}} = \frac{1}{4ab} \int_{-a}^{a} \int_{-b}^{b} p_\zeta(x) e^{-j(n\frac{\pi}{a}x + m\frac{\pi}{b}y)} dxdy, \tag{14a}$$

$$\bar{q}^{(o)}_{\zeta_{(n,m)}} = \frac{1}{4ab} \int_{-a}^{a} \int_{-b}^{b} q_\zeta(x) e^{-j(n\frac{\pi}{a}x + m\frac{\pi}{b}y)} dxdy, \tag{14b}$$

and the matrices $\mathbf{P^{(1)}}$ and $\mathbf{Q^{(1)}}$ are defined as:

$$\mathbf{P^{(1)}} = \left(\mathbf{I} + \mathbf{P^{(0)}}\right), \qquad \mathbf{Q^{(1)}} = \left(\mathbf{I} + \mathbf{Q^{(0)}}\right), \tag{14c, d}$$

where $\mathbf{I}$ is the unity matrix.

Equations (12a), (12b) and (12c) are rewritten in a matrix form as follows

$$\begin{aligned} &\mathbf{K^{(0)}} E_x + \frac{k_o^2 \chi_0}{2s} \mathbf{Q^{(1)}} \mathbf{G} E_x + \frac{jk_{ox}}{2s} \mathbf{Q^{(1)}} \mathbf{N} \left(\mathbf{G_x} E_x + \mathbf{G_y} E_y\right) \\ &- \frac{1}{2sR^2} E_x - \frac{1}{R} E_\zeta + \mathbf{Q^{(0)}} \mathbf{K1^{(0)}} E_x + \frac{1}{2sR} jk_{ox} \mathbf{P^{(1)}} \mathbf{N} E_x \\ &= \hat{E}_{x_0} - \frac{1}{sR} \hat{E}_{\zeta_0}, \end{aligned} \tag{15a}$$

$$\begin{aligned} &\mathbf{K^{(0)}} E_y + \frac{k_o^2 \chi_0}{2s} \mathbf{Q^{(1)}} \mathbf{G} E_y + \frac{jk_{oy}}{2s} \mathbf{Q^{(1)}} \mathbf{M} \left(\mathbf{G_x} E_x + \mathbf{G_y} E_y\right) \\ &+ \mathbf{Q^{(0)}} \mathbf{K1^{(0)}} E_y + \frac{1}{2sR} jk_{ox} \mathbf{P^{(1)}} \mathbf{N} E_y \\ &= \hat{E}_{y_0}, \end{aligned} \tag{15b}$$

$$\begin{aligned} &\mathbf{K^{(0)}} E_\zeta + \frac{k_o^2 \chi_0}{2s} \mathbf{Q^{(1)}} \mathbf{G} E_\zeta + \frac{1}{2} \mathbf{Q^{(1)}} \left(\mathbf{G_x} E_x + \mathbf{G_y} E_y\right) - \frac{1}{2sR^2} E_\zeta \\ &+ \frac{1}{R} E_\zeta + \mathbf{Q^{(0)}} \mathbf{K1^{(0)}} E_\zeta + \frac{1}{2sR} jk_{ox} \mathbf{P^{(1)}} \mathbf{N} E_\zeta \\ &= \hat{E}_{\zeta_0} + \frac{1}{sR} E_{\zeta_0} + \frac{1}{2s} \mathbf{Q^{(1)}} \left(\mathbf{G_x} E_{x_0} + \mathbf{G_y} E_{y_0}\right), \end{aligned} \tag{15c}$$

where the initial-value vectors $\hat{E}_{x_0}$, $\hat{E}_{y_0}$, and $\hat{E}_{\zeta_0}$ are defined from the terms $(s\bar{E}_{x_0} + \bar{E}'_{x_0})/2s$, $(s\bar{E}_{y_0} + \bar{E}'_{y_0})/2s$, and $(s\bar{E}_{\zeta_0} + \bar{E}'_{\zeta_0})/2s$, respectively.

The diagonal matrices $\mathbf{K^{(0)}}$, $\mathbf{M}$ and $\mathbf{N}$ were defined in Ref. [12]. The metric coefficient h_ζ is dependent on x ($h_\zeta = 1 + x/R$). Thus the next diagonal matrix $\mathbf{K^{(1)}}$ is defined as

$$K^{(1)}_{(n,m)(n',m')} \left\{ \left[k_o^2 - (n\pi/a)^2 - (m\pi/b)^2 \right] /2s \right\} \delta_{nn'}\delta_{mm'}, \tag{16}$$

where $\delta_{nn'}$ and $\delta_{mm'}$ are the Kronecker delta functions.

The modified wave-number matrices are defined as

$$\mathbf{D_x} \equiv \mathbf{K^{(0)}} + \mathbf{Q^{(0)}K1^{(0)}} + \frac{k_o^2\chi_0}{2s}\mathbf{Q^{(1)}G} + \frac{jk_{ox}}{2s}\mathbf{Q^{(1)}NG_x} + \frac{1}{2sR}jk_{ox}\mathbf{P^{(1)}N} - \frac{1}{2sR^2}\mathbf{I}, \tag{17a}$$

$$\mathbf{D_y} \equiv \mathbf{K^{(0)}} + \mathbf{Q^{(0)}K1^{(0)}} + \frac{k_o^2\chi_0}{2s}\mathbf{Q^{(1)}G} + \frac{1}{2sR}jk_{ox}\mathbf{Q^{(1)}N} + \frac{jk_{oy}}{2s}\mathbf{P^{(1)}MG_y}, \tag{17b}$$

$$\mathbf{D}_\zeta \equiv \mathbf{K^{(0)}} + \mathbf{Q^{(0)}K1^{(0)}} + \frac{k_o^2\chi_0}{2s}\mathbf{Q^{(1)}G} + \frac{1}{2sR}jk_{ox}\mathbf{P^{(1)}N} + \frac{1}{R}\mathbf{I} - \frac{1}{2sR^2}\mathbf{I}. \tag{17c}$$

Thus Eqs. (15a) to (15c) result in

$$\mathbf{D_x}E_x = \hat{E}_{x_0} - \frac{jk_{ox}}{2s}\mathbf{Q^{(1)}NG_y}E_y - \frac{1}{sR}\hat{E}_{\zeta_0} + \frac{1}{R}E_\zeta, \tag{18a}$$

$$\mathbf{D_y}E_y = \hat{E}_{y_0} - \frac{jk_{oy}}{2s}\mathbf{Q^{(1)}MG_x}E_x, \tag{18b}$$

$$\mathbf{D}_\zeta E_\zeta = \hat{E}_{\zeta_0} + \frac{1}{2s}\mathbf{Q^{(1)}}\left(\mathbf{G_x}E_{x_0} + \mathbf{G_y}E_{y_0}\right) - \frac{1}{2}\mathbf{Q^{(1)}}\left(\mathbf{G_x}E_x + \mathbf{G_y}E_y\right) + \frac{1}{sR}E_{\zeta_0}. \tag{18c}$$

After some algebraic steps, the components of the electric field are formulated as follows:

$$E_x = \left\{ \mathbf{D_x} + \alpha_1\mathbf{Q^{(1)}M_1Q^{(1)}M_2} + \frac{1}{R}\mathbf{D}_\zeta^{-1}\left(-\frac{1}{2}\mathbf{Q^{(1)}G_x} + \frac{1}{2}\alpha_2\mathbf{Q^{(1)}M_3Q^{(1)}M_2}\right)\right\}^{-1}\left(\hat{E}_{x_0} - \frac{1}{sR}\hat{E}_{\zeta_0} - \alpha_3\mathbf{Q^{(1)}M_1}\hat{E}_{y_0}\right.$$

$$+\frac{1}{R}\mathbf{D}_{\zeta}^{-1}\left(\hat{E}_{\zeta_0}+\frac{1}{sR}E_{\zeta_0}+\frac{1}{2s}\mathbf{Q^{(1)}}(\mathbf{G_x}E_{x_0}+\mathbf{G_y}E_{y_0})-\frac{1}{2}\mathbf{Q^{(1)}}\mathbf{M_3}\hat{E}_{y_0}\right)\Bigg), \tag{19a}$$

$$E_y = \mathbf{D_y}^{-1}\left(\hat{E}_{y_0}-\frac{jk_{oy}}{2s}\mathbf{Q^{(1)}}\mathbf{M}\mathbf{G_x}E_x\right), \tag{19b}$$

$$E_\zeta = \mathbf{D}_{\zeta}^{-1}\left\{\hat{E}_{\zeta_0}+\frac{1}{2s}\mathbf{Q^{(1)}}\left(\mathbf{G_x}E_{x_0}+\mathbf{G_y}E_{y_0}\right)\right.$$
$$\left.-\frac{1}{2}\mathbf{Q^{(1)}}\left(\mathbf{G_x}E_x+\mathbf{G_y}E_y\right)+\frac{1}{sR}E_{\zeta_0}\right\}, \tag{19c}$$

where

$$\alpha_1=\frac{k_{ox}k_{oy}}{4s^2},\qquad \alpha_2=\frac{jk_{oy}}{2s},\qquad \alpha_3=\frac{jk_{ox}}{2s},$$
$$\mathbf{M_1}=\mathbf{N}\mathbf{G_y}\mathbf{D_y}^{-1},\qquad \mathbf{M_2}=\mathbf{M}\mathbf{G_x},\qquad \mathbf{M_3}=\mathbf{G_y}\mathbf{D_y}^{-1}.$$

These equations describe the transfer relations between the spatial spectrum components of the output and input waves in the dielectric waveguide. Similarly, the other components of the magnetic field are obtained.

The transverse field profiles are computed by the inverse Laplace and Fourier transforms, as follows

$$E_y(x,y,\zeta)=\sum_n\sum_m\int_{\sigma-j\infty}^{\sigma+j\infty}E_y(n,m,s)e^{jnk_{ox}x+jmk_{oy}y+s\zeta}ds. \tag{20a}$$

The inverse Laplace transform is performed in this study by a direct numerical integration on the s-plane by the method of Gaussian Quadrature. The integration path in the right side of the s-plane includes all the singularities, as proposed by Salzer [14, 15]

$$\int_{\sigma-j\infty}^{\sigma+j\infty}e^{s\zeta}E_y(s)ds=\frac{1}{\zeta}\int_{\sigma-j\infty}^{\sigma+j\infty}e^{p}E_y(p/\zeta)dp=\frac{1}{\zeta}\sum_{i=1}^{15}w_iE_y(s=p_i/\zeta), \tag{20b}$$

where w_i and p_i are the weights and zeros, respectively, of the orthogonal polynomials of order 15. The Laplace variable s is normalized by p_i/ζ in the integration points, where $\mathrm{Re}(p_i)>0$ and all the poles should be localized in their left side on the s-plane. This approach of a direct integral transform does not require as other methods to deal with each singularity separately.

The ζ component of the average-power density of the complex Poynting vector is given by

$$S_{av} = \frac{1}{2}\mathrm{Re}\left\{E_x H_y^* - E_y H_x^*\right\}, \tag{21}$$

where the asterisk indicates the complex conjugate. The active power is equal to the real part of the complex Poynting vector.

A Fortran code is developed using NAG subroutines [16]. Several examples computed on a Unix system are presented in the next section.

It is very interesting to compare between this proposed mode model for the wave propagation in uniform curved waveguide with a rectangular cross section and the method for the propagation in uniform curved waveguide with a circular cross section [13]. The similar main points are:

(1). The calculations in both mode model methods are based on using Laplace transform, and the output fields are computed by the inverse Laplace transform.

(2). The objective in both above methods was to develop a mode model in order to provide a numerical tool for the calculation of the output fields also for uniform curved waveguides. We took into account all the terms (namely, up to the fourth order of $1/R$, where the further orders are equal zero) in the calculations, without neglecting the terms of the bending. This means that we have polynomial expressions of order four.

The technique of the two above methods is quite different. The proposed technique in this study for a rectangular cross section is based on Fourier coefficients of the transverse dielectric profile and those of the input wave profile. On the other hand, the technique for a circular cross section in Ref. [13] was based on the development of the longitudinal components of the fields into Fourier-Bessel series. The transverse components of the fields were expressed as functions of the longitudinal components in the Laplace plane and were obtained by using the inverse Laplace transform.

4. EXAMPLES OF THIS MODE MODEL

This section presents several examples which demonstrate features of the proposed mode model derived in the previous section. The method of this model is based on Fourier coefficients, thus the accuracy of the method is depended on the number of the modes in the system. Further we assume $N = M$. The practical use of a dielectric slab is given in Ref. [12]. Further the next examples will demonstrate the results of

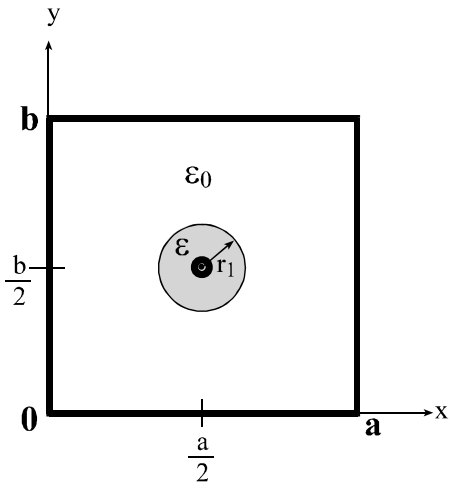

Figure 2. An example of the cross-section of a dielectric profile loaded rectangular waveguide.

the solutions in the case of a circular dielectric profile in a rectangular waveguide (Fig. 2) for a millimeter-wave regime. Figure 2 give us good example for inhomogeneous dielectric profile in the cross-section. The refractive index of the core (dielectric profile) is greater than that of the cladding (air).

According to the TMF method [12] we have two ways to compare between the results of our mode model and the another known model (analytical method), as follows:

1. Comparison between the output fields for every order ($N = 1, 3, 5, 7,$ and 9) to the another known method (analytical method).
2. Comparison between the output fields (according to our model) for every two orders ($N = 1, 3$, $N = 3, 5$, $N = 5, 7$, and $N = 7, 9$). This way is efficient in the cases that we have complicated problems that we can't compare with another known method.

Example:

The test-case for the straight waveguide is obtained by letting $R \to \infty$ (the coordinate ζ is changed to z). The comparison between this test-case of our mode model to the known transcendental equation as a benchmark and the solutions of the fields were demonstrated by TMF results [12] for every order ($N = 1, 3, 5, 7,$ and 9). The limit of the convergence between $N = 5$ and the analytical method results was 0.699%. Additionally, the limit of the convergence between $N = 9$

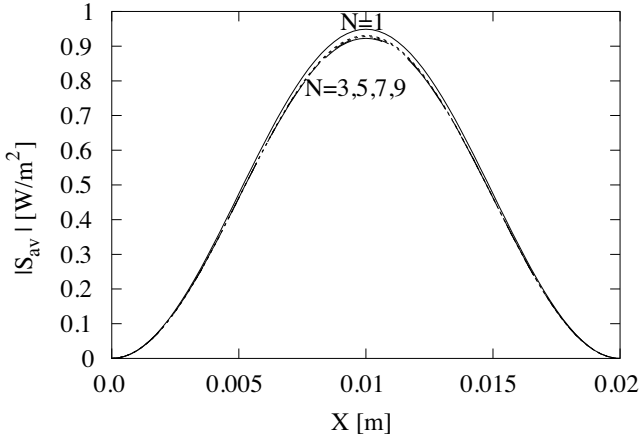

Figure 3. A solution of the output power density ($|S_{av}|$) as a response to a TE_{10} input wave and a circular dielectric profile for $N = 1, 3, 5, 7,$ and 9, where $a = b = 2\,\text{cm}$, $r1 = 0.5\,\text{mm}$, $z = 20\,\text{cm}$, $\lambda = 3.75\,\text{cm}$, $y = b/2$, and $\epsilon_r = 2.25$.

and the analytical method results was 0.0827%. The limit of the convergence between $N = 7$ and $N = 9$ was 0.196%. A convergence less than 1% was achieved in this example for $N \geq 5$. The model was convergenced by five steps ($N = 1, 3, 5, 7,$ and 9). The number of the modes is equal to $(2N + 1)^2$. For $N = 7$ and $N = 9$ the number of the modes was equal to 225. This comparison confirms the validity of the mode model.

A circular dielectric profile in a rectangular waveguide

The geometrical shape of a circular dielectric profile loaded rectangular waveguide is demonstrated in Fig. 2 for inhomogeneous profile in the cross-section. The output power density (S_{av}) as a response to a TE_{10} input wave and a circular dielectric profile is shown in Fig. 3 for $N = 1, 3, 5, 7,$ and 9, where $y = b/2$ and $R \to \infty$. When N is increases, then $S_{av}(N)$ approaches S_{av}.

In this example the length (z) of the straight waveguide is 20 cm, and the radius ($r1$) of a circular dielectric profile is 0.5 mm (Fig. 2). The next parameters are $a = b = 2\,\text{cm}$, $\epsilon_r = 2.25$, and $\lambda = 3.75\,\text{cm}$. A solution of the output power density ($|S_{av}|$) as a response to a TE_{10} input wave and a circular dielectric profile is shown in Fig. 3 for $N = 1, 3, 5, 7,$ and 9. The output transverse profile of the output power density ($|S_{av}|$) as a response to a TE_{10} input wave and a circular dielectric profile is shown in Fig. 4 for the same above parameters.

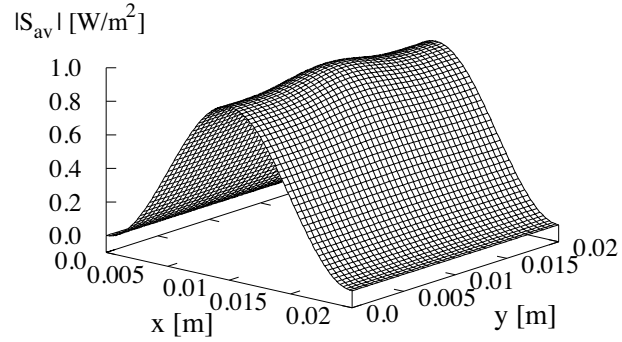

Figure 4. A solution of the output power density ($|S_{av}|$) as a response to a TE_{10} input wave and a circular dielectric profile where $a = b = 2\,\text{cm}$, $r1 = 0.5\,\text{mm}$, $z = 20\,\text{cm}$, $\lambda = 3.75\,\text{cm}$, and $\epsilon_r = 2.25$.

Further the convergence of the solution is verified by the criterion

$$C(N) \equiv \log\left\{\frac{\max\left(\left|S_{av}^{N+2} - S_{av}^{N}\right|\right)}{\left|\max\left(S_{av}^{N+2}\right) - \min\left(S_{av}^{N}\right)\right|}\right\}, \qquad N \geq 1. \tag{22}$$

where the number of the modes is equal to $(2N+1)^2$. The order N determines the accuracy of the solution. If the value of the criterion is less then -2, then the numerical solution is well convergenced.

The convergence of the output transverse profile of the power density as a response to a TE_{10} input wave and a circular dielectric profile is shown in Fig. 5. When N is increases, then $S_{av}(N)$ approaches S_{av}. The value of the criterion between $N = 7$ and $N = 9$ is equal to $-2.8 \simeq -3$, namely a thousandth part.

The output fields are dependent on the input wave profile (TE_{10} mode) and the dielectric profile. By changing the value of the parameter ϵ_r of the core in the cross-section (Fig. 2) as regard to the cladding (air) from 2.25 to 10, the output transverse profile of the power density (S_{av}) is changed. For small values of ϵ_r (e.g., $\epsilon_r = 2.25$) the half-sine (TE_{10}) shape of the output power density appears (Fig. 4), with a little influence of the Gaussian shape. On the other hand, for large values of ϵ_r (e.g., $\epsilon_r = 10$) the Gaussian shape of the output power density appears (Fig. 6), with a little influence of the half-sine (TE_{10}) shape. The behavior of the Gaussian shape (Fig. 6) is similar to another theoretical result for hollow waveguide [13] in the range of the IR regime. The above examples demonstrate the influence of the dielectric profile for inhomogeneous cross section. In this way, one can

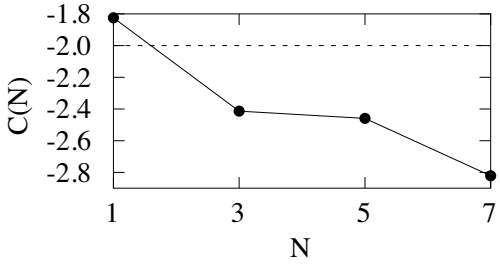

Figure 5. The convergence of the of the output power density $N = 1 - 7$, where $a = b = 2\,\text{cm}$, $r1 = 0.5\,\text{mm}$, $z = 20\,\text{cm}$, $\lambda = 3.75\,\text{cm}$, and $\epsilon_r = 2.25$.

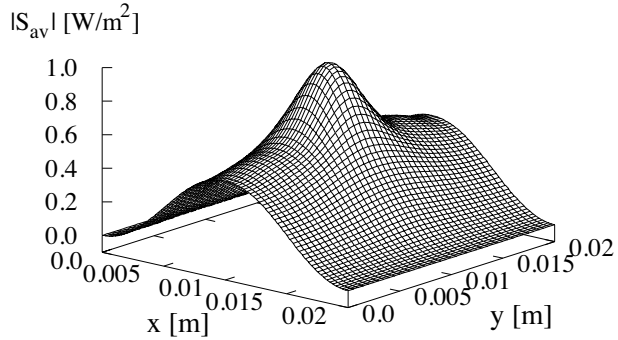

Figure 6. A solution of the output power density ($|S_{av}|$) as a response to a TE_{10} input wave and a circular dielectric profile for where $a = b = 2\,\text{cm}$, $r1 = 0.5\,\text{mm}$, $z = 20\,\text{cm}$, $\lambda = 3.75\,\text{cm}$, and $\epsilon_r = 10$.

solve problems for an arbitrary dielectric profile in the cross section.

One of the parameters that we studied was the output power transmission as a function of the radius of curvature where the waveguide's cross-section is given in Fig. 2. The dependence of the power transmission as a function of the bending $(1/R)$ is shown in Fig. 7, where R is the radius of the bending. For small values of $1/R$ the power transmission is large and decreases with increasing the bending $(1/R)$. The behavior of this result (Fig. 7) is similar to other theoretical results for hollow waveguide [13, 17] in the range of the IR regime.

This example demonstrates the influence of the bending on the power transmission where we take into account all the terms in the calculations without neglecting the terms of the bending (namely, up to the fourth order of $1/R$, where the further orders are equal zero).

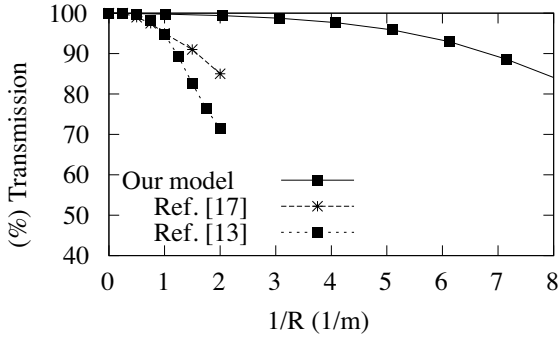

Figure 7. The output power transmission as a function of the radius of curvature for $\zeta = 20\,\mathrm{cm}$, where $a = b = 2\,\mathrm{cm}$, $r1 = 0.5\,\mathrm{mm}$, $\epsilon_r = 2.25$ and $\lambda = 3.75\,\mathrm{cm}$.

The calculations are depended on h_ζ, h_ζ^2, h_ζ^3 and h_ζ^4 ($h_\zeta = 1 + x/R$), where h_ζ is the metric coefficient. Thus the maximum value of the bending in the calculations is of the order of $1/R^4$. This will enable us to understand more precisely the influence of the bending on the output fields, output power density, and output power transmission. The results of the solutions of the output fields, output power density, and output power transmission are obtained for a radius of curvature $0.1\,\mathrm{m} \leq R \leq \infty$.

This model can take into account the cases of smaller R only if the step's angle (δ_p) is very small, where the condition is given according to $\delta_p \geq (2a)/(2\pi R)$ (Eq. (A2), in Appendix A).

5. CONCLUSIONS

The objective of this work was to generalize the method [12] also for a curved dielectric waveguide. Another objective was to demonstrate the ability of the model to solve practical problems with inhomogeneous dielectric profiles. A theoretical mode model was developed to provide a numerical tool for the calculation of the output fields, output power density, and output power transmission for radius of curvature $0.1\,\mathrm{m} \leq R \leq \infty$. Therefore we took into account all the terms (namely, up to the fourth order of $1/R$, where the further orders are equal zero) in the calculations. Note that all the terms were taken into account without neglecting the terms that belong to the bending. The calculations are depended on h_ζ, h_ζ^2, h_ζ^3 and h_ζ^4 ($h_\zeta = 1 + x/R$), where h_ζ is the metric coefficient. Thus the maximum value of the bending in the calculations is of the order of $1/R^4$. This will enable us to understand more precisely

the influence of the bending on the output fields, output power density, and output power transmission of curved waveguides. The propagation of the electromagnetic wave along the curved waveguide is computed by *input-output* relations (Eqs. (19)).

The mode model was developed in order to predict the output power transmission as a function of the curvature for a given ζ. For small values of $1/R$ the output power transmission is large and decreases with increasing the bending $(1/R)$. The behavior of the result is similar to other theoretical results for hollow waveguide [13, 17] in the range of the IR regime.

The test-case for the straight waveguide was obtained by letting $R \to \infty$ (the coordinate ζ is changed to z). The comparison between this test-case of our mode model to the known transcendental equation as a benchmark and the solutions of the fields were demonstrated in Ref. [12]. The examples in this paper were demonstrated in the case of a circular dielectric profile in a rectangular waveguide (Fig. 2) for a millimeter-wave regime. This geometrical shape in the cross section was demonstrated for inhomogeneous dielectric profile. In this case the refractive index of the core (dielectric profile) is greater than that of the cladding (air). By changing the value of the parameter ϵ_r of the core in the cross-section (Fig. 2) as regard to the cladding (air) from 2.25 to 10, the output transverse profile of the power density (S_{av}) is changed. For small values of ϵ_r (e.g., $\epsilon_r = 2.25$) the half-sine (TE_{10}) shape of the output power density appears (Fig. 4), with a little influence of the Gaussian shape. On the other hand, for large values of ϵ_r (e.g., $\epsilon_r = 10$) the Gaussian shape of the output power density appears (Fig. 6), with a little influence of the half-sine (TE_{10}) shape. The behavior of the Gaussian shape (Fig. 6) is similar to another theoretical result for hollow waveguide [13] in the range of the IR regime. The above examples demonstrate the influence of the dielectric profile for inhomogeneous cross section. In this way, one can solve problems for an arbitrary dielectric profile in the cross section.

This model can take into account the cases of smaller R only if the step's angle (δ_p) is very small, where the condition is given according to $\delta_p \geq (2a)/(2\pi R)$ (Eq. (A2), in Appendix A).

This mode model might be a useful tool for the analysis of continuous and discontinuous dielectric waveguides in the microwave and millimeter-wave regimes, for diffused optical waveguides in integrated optics, and IR regime.

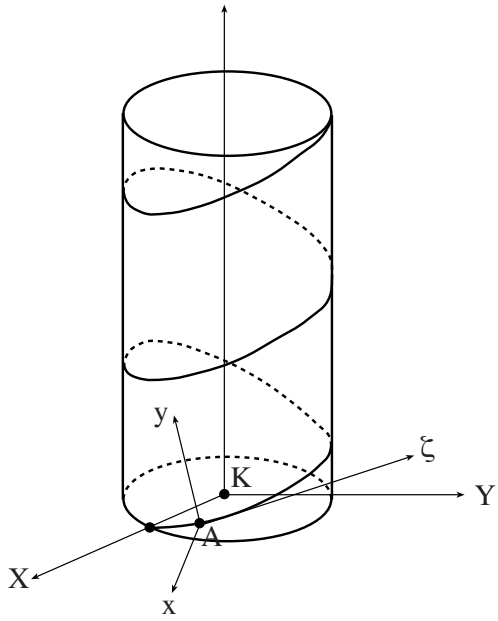

Figure A1. The transformation of the orthogonal system (x, y, ζ) from point A to the orthogonal system (X, Y, Z) at point K.

APPENDIX A.

By using Laplace transform, the fields at $\zeta = \infty$ are zero. Therefore the ζ axis of the curved waveguide is a rectangular helix, as shown in Fig. A1. By rotations and translation of the orthogonal system (x, y, ζ) from point A to the orthogonal system (X, Y, Z) at point K and using a small step's angle δ_p, the curved waveguide transformation of the coordinates is given by

$$X = (R + x)\cos\left(\frac{\zeta}{R}\right) + y\sin(\delta_p)\sin\left(\frac{\zeta}{R}\right), \tag{A1a}$$

$$Y = (R + x)\sin\left(\frac{\zeta}{R}\right) - y\sin(\delta_p)\cos\left(\frac{\zeta}{R}\right), \tag{A1b}$$

$$Z = y + \zeta\sin(\delta_p). \tag{A1c}$$

For small values of the step angle δ_p, the condition is given by

$$\delta_p > \frac{2a}{2\pi R}. \tag{A2}$$

The metric coefficients according to Eqs. (A1a) to (A1c) are

$$h_x = 1, \tag{A3a}$$

$$h_y = \sqrt{1 + (\delta_p)^2}, \tag{A3b}$$

$$h_\zeta = \sqrt{\frac{1}{R^2}(R+x)^2 + (\delta_p)^2\left(1 + \left(\frac{y}{R}\right)^2\right)}. \tag{A3c}$$

Further we take in account small values of δ_p angles. For instance, if the value of the cross-section's dimension (a) is 20 mm and the bending radius (R) is 0.5 m, then the value of the step's angle (A2) is small, and the value of $(\delta_p)^2$ is negligible ($(\delta_p)^2 \simeq 1.62 \times 10^{-4} \ll 1$). Thus the metric coefficients as given in Eqs. (2a) to (2c) are justified. The model in this paper can take into account the cases of smaller R only if the step angle (δ_p) is very small, where the condition is given in Eq. (A2).

REFERENCES

1. Riess, K., "Electromagnetic waves in a bent pipe of rectangular cross-section," *Q. Appl. Math.*, Vol. 1, 328–333, 1944.
2. Rice, S. O., "Reflections from circular bends in a rectangular wave guides-matrix theory," *Bell Syst. Tech. J.*, Vol. 27, 305–349, 1948.
3. Heiblum, M. and J. H. Harris, "Analysis of curved optical waveguides by conformal transformation," *IEEE J. Quantum Electron.*, Vol. 11, 75–83, 1975, Correction, ibid., Vol. 12, 313, 1976.
4. Kawakami, S., M. Miyagi, and S. Nishida, "Bending losses of dielectric slab optical waveguide with double or multiple claddings," *Appl. Optics*, Vol. 14, 2588–2597, 1975. Correction, ibid., Vol. 15, 1681, 1976.
5. Chang, D. C. and F. S. Barnes, "Reduction of radiation loss in a curved dielectric slab waveguide," Sci. Rept. 2 AFOSR-72-2417, 1973.
6. Marcatily, E. A. J. and R. A. Schmeltzer, "Hollow metallic and dielectric waveguides for long distance optical transmission and lasers," *Bell Syst. Tech. J.*, Vol. 43, 1783–1809, 1964.
7. Cochran, J. A. and R. G. Pecina, "Mode propagation in continuously curved waveguides," *Radio Science*, Vol. 1 (new series), No. 6, 679–696, 1966.
8. Carle, P. L., "New accurate and simple equivalent circuit for

circular E-plane bends in rectangular waveguide," *Electronics Letters*, Vol. 23, No. 10, 531–532, 1987.

9. Weisshaar, A., S. M. Goodnick, and V. K. Tripathi, "A rigorous and efficient method of moments solution for curved waveguide bends," *IEEE Trans. Microwave Theory Tech.*, Vol. MTT-40, No. 12, 2200–2206, 1992.
10. Cornet, P., R. Duss'eaux, and J. Chandezon, "Wave propagation in curved waveguides of rectangular cross section," *IEEE Trans. Microwave Theory Tech.*, Vol. MTT-47, 965–972, 1999.
11. Lewin, L., D. C. Chang, and E. F. Kuester, *Electromagnetic Waves and Curved Structures*, Chap. 8, 95–113, Peter Peregrinus Ltd., 1977.
12. Menachem, Z. and E. Jerby, "Transfer matrix function (TMF) for wave propagation in dielectric waveguides with arbitrary transverse profiles," *IEEE Trans. Microwave Theory Tech.*, Vol. MTT-46, 975–982, 1998.
13. Menachem, Z., N. Croitoru, and J. Aboudi, "Improved mode model for IR wave propagation in a toroidal dielectric waveguide and applications," *Opt. Eng.*, Vol. 41, 2002.
14. Salzer, H. E., "Orthogonal polynomials arising in the numerical evaluation of inverse Laplace transforms," *Math. Tables and Other Aids to Comut.*, Vol. 9, 164–177, 1955.
15. Salzer, H. E., "Additional formulas and tables for orthogonal polynomials originating from inversion integrals," *J. Math. Phys.*, Vol. 39, 72–86, 1961.
16. The Numerical Algorithms Group (NAG) Ltd., Wilkinson House, Oxford, U.K.
17. Croitoru, N., D. Mendlovic, J. Dror, S. Ruschin, and E. Goldenberg, "Improved metallic tube infrared waveguides with inside dielectric coating," *Proc. Soc. Photo-Opt. Instrum. Eng.*, Vol. 713, 6–11, 1986.